ISSN (Print) 1226-1750
ISSN (Online) 2233-6656
Journal of Magnetics 28(3), 251-257 (2023) https://doi.org/10.4283/JMAG.2023.28.3.251

Effect of Various Composition Ratios on the Exchange Spring Effect in $SrFe_{12}O_{19}/CoFe_2O_4$ Nanocomposite Magnets

Novrita Idayanti[1]*, Dedi[1], Dadang Mulyadi[1], Tony Kristiantoro[1], Nanang Sudrajat[1], Gandi Sugandi[1], and Azwar Manaf[2]

[1]*Research Center for Electronics, National Research and Innovation Agency, Bandung West Java, Indonesia*
[2]*Department of Physics, Universitas Indonesia, Depok West Java, Indonesia*

(Received 20 October 2022, Received in final form 27 June 2023, Accepted 27 June 2023)

This study aims to examine the effect of various composition ratios on the exchange spring effect of strontium ferrite ($SrFe_{12}O_{19}$)/cobalt ferrite ($CoFe_2O_4$) nanocomposite magnets. Nanoparticles of hexagonal hard phase $SrFe_{12}O_{19}$ and spinel soft phase $CoFe_2O_4$ were each prepared through mechanical alloying and high-power ultrasonic irradiation processes. Furthermore, the constituent of the hard-soft particles was weighed based on its ratios and the mixture was homogenized under a sonicator-type Qsonica at a frequency of 20 kHz for an hour. The bulk composite samples were obtained in cylindrical pellets form through compaction of mixture powders at 5000 kg/cm^2, followed by sintering at 1200 °C. The exchange spring effect enhanced the magnetic properties, surpassing the normal limit for non-interacting magnetic particles due to enhanced grain interactions. The results showed that the degree of property enhancement depended on the various composition ratios and microstructure of the composite magnets. The magnetization of saturation (M_s) of the samples increased compared to a single $SrFe_{12}O_{19}$. Furthermore, the highest coercivity (H_c) and product energy maximum $(BH)_{max}$ values were observed in the sample which had mass ratios of SHF:COF of 85:15 with coded S80C20. The occurrence of exchange spring effects was observed in material characterized by a microstructure consisting of a hard-magnetic phase with elevated magnetocrystalline anisotropy and saturation magnetization values, along with a soft magnetic phase exhibiting high saturation magnetization value.

Keywords : exchange spring magnet, nanocomposite, $SrFe_{12}O_{19}$, $CoFe_2O_4$

1. Introduction

Nanocomposite permanent magnets are innovative magnetic materials that combine both hard and soft magnetic phases, thereby improving remanence and maximum energy products. This enhancement is achieved through the utilization of exchange springs between the two magnetic phases, and this is made possible by the nanocrystalline structure [1, 2]. According to theoretical calculations, the maximum energy product, $(BH)_{max}$ of a permanent nanocomposite magnet is 954 kJ/m^3 (120 MGOe) [3]. This figure represents a significant improvement compared to the leading sintered NdFeB magnets, which have a maximum energy of 445 kJ/m^3 (56 MGOe), effectively doubling their performance [4, 5].

The exchange spring effect can be achieved in materials with a microstructure that comprises a hard-magnetic phase possessing high magnetocrystalline anisotropy and saturation magnetization values, along with a soft magnetic phase exhibiting high saturation magnetization value. In this composite structure, both phases are effectively exchange-coupled, leading to enhanced magnetic properties compared to those of a single-phase magnet. The hard-magnetic phase, characterized by its high magnetocrystalline anisotropy, contributes to a high coercivity (H_c), while the soft magnetic phase contributes a high magnetization value [1]. The combination of these phases within the composite magnet increases the value of remanence magnetization (M_r), saturation magnetization (M_s), and $(BH)_{max}$ [2]. Several studies have been carried out in this field with varying results. Liu *et al*. reported the synthesis of $Ba_{0.5}Sr_{0.5}Fe_{12}O_{19}$ and $Y_3Fe_5O_{12}$ using the sol-gel auto-combustion method, which showed better homogeneity and exchange coupling effects [6]. Furthermore, Radmanesh *et al.* [3] examined the effect of grain size on exchange-

*Corresponding author: Tel: +62-22-6037707
e-mail: novrita13@gmail.com

coupled oxides, focusing on $SrFe_{12}O_{19}/Ni_{0.7}Zn_{0.3}Fe_2O_4$ oxide-based nanocomposites. The magnetic properties observed in these studies revealed the presence of concave hysteresis loops due to non-complete exchange coupling at the interfaces of hard and soft ferrites. When the grain size of the soft phase is the same as the hard phase, the dipolar interaction becomes dominant and the magnetic behavior of hard/soft nanocomposites is similar to that of two-phase uncoupled magnets. H. Nikmanesh *et al*. [4] studied strontium hexaferrite and nickel nano-composite ferrite synthesized using the sol-gel method. The results demonstrated superior performance when compared to the mixture of strontium hexaferrite and zinc-nickel ferrite as a hard and soft phase, respectively. The variation of the coercivity, saturation magnetization, and the ratio of remanence to saturation magnetization (M_r/M_s) with respect to the hard-to-soft weight ratio can be best explained by considering the interplay of exchange and dipole interactions in the nanocomposites.

For optimal effectiveness of exchange-spring coupling, it is crucial that the two phases are in close contact, and the grain size of the soft phase must be twice the domain wall width of the hard magnetic aspect [5, 7]. The magnetic characteristics of exchange spring magnets are strongly influenced by the microstructure, grain size, purity level, and the distribution of the hard and soft phases [8]. Therefore, the composition plays a significant role in determining the occurrence and effectiveness of exchange-spring behavior. Improved magnetic properties have been observed in composite magnets, highlighting the impact of composition on exchange spring magnets. Yin *et al*. [9] studied the effect of partial Mo substitution for Fe in the phase composition of $Nd_8Fe_{86-x}Mo_xB_6$ (x = 0, 1, 2, and 3). The results showed remanence enhancement due to the effect of exchange coupling between the hard magnetic phase and soft magnetic α-Fe, leading to decreased H_c. The report also revealed that the substitution of Mo for Fe was found to increase the H_c and decrease $(BH)_{max}$. Furthermore, Yang *et al*. [10] observed the composition dependence of the magnetic properties of $CoFe_2O_4/CoFe_2$ composites. A significant increase was observed in the saturation magnetization of the composite magnet, along with an increment in the volume fraction of soft-magnetic $CoFe_2$. The enhancement of the inter-phase exchange coupling occurred when the soft-magnetic $CoFe_2$ nano-particles were increased. The nanocomposite ceramics of $CoFe_2O_4/CoFe_2$ have potential usage in the field of information technology, while the exchange-spring magnet in hard-soft magnetic composite materials has wide applications [11]. Therefore, this study aims to examine the effect of various composition ratios of $SrFe_{12}O_{19}$ (SHF) and $CoFe_2O_4$ (COF) on the influence of exchange springs magnet. The composition of the hard and soft phases plays a crucial role in determining the exchange behavior of the composite magnetic spring. The hard-magnetic phase, characterized by its high magnetocrystalline anisotropy, contributes to a high coercivity (H_c), while the soft magnetic phase provides a high magnetization of saturation (M_s).

This study utilized a distinct method, differing from the approaches mentioned in the references and previous reports. The method employed in this study involved a combination of mechanical alloying and high-power ultrasonic irradiation.

2. Materials and Methods

2.1. Materials

All the raw materials used in the synthesis were of analytical grade without further purification. Iron oxide, Fe_2O_3 (E-Merck, 99%) and strontium carbonate, $SrCO_3$ (E-Merck, 99%) were reacted together for the preparation of SHF, while Fe_2O_3 was combined with cobalt carbonate, $CoCO_3$ (E-Merck, 98%) to produce COF. Some of the additives used in the synthesis of SHF included silicon oxide (SiO_2) and calcium oxide (CaO), while COF was prepared without additives.

The synthesis procedure in this study was divided into three steps, including the preparation of SHF powder, COF, and nanocomposite SHF/COF.

2.2. Synthesis of SHF and COF

The synthesized hard SHF and soft magnetic COF were prepared separately using mechanical alloying methods. SHF was synthesized using the stoichiometry raw material amounts of Fe_2O_3 and $SrCO_3$, which were mixed in a tumbler ball milling type containing 50 pieces of stainless steel balls at a mass ratio of 1:10. The milling process was carried out for 8 hours in a wet condition of alcohol. Subsequently, the mixtures were dried at 100 °C in the furnace for approximately 2 hours and then calcined at 1200 °C for 3 hours, leading to the formation of SHF crystalline materials. The calcined powder was then re-milled for 16 hours, with the addition of SiO_2 and CaO. The powder was sintered at 1250 °C for 1 hour and SHF powder was ready to be composited.

COF was synthesized from raw materials, namely Fe_2O_3 and $CoCO_3$ powder, which were mixed in a ball milling machine for 10 hours in a wet condition of alcohol. The powder was calcined at 1000 °C for 2 hours and then sintered at the same temperature and holding time of calcination.

2.3. Synthesis of nanocomposite SHF/COF

The nanocomposite powder SHF/COF was prepared with varying mass composition ratios between SHF and COF. The samples coded S70C30, S75C25, S80C20, and S85C15 had mass ratios of SHF:COF of 70:30, 75:25, 80:20, and 85:15, respectively. A total of 30 g of the mixture powders were each dissolved in 300 ml of distillate water and irradiated ultrasonically at a frequency of 20 kHz for 1 hour. After the ultrasonic process, the nanoparticle powder formed was well mixed and dispersed. Subsequently, the powder mixture was dried at 100 °C, and 3.5 of the sample was inserted into a cylindrical die of 12 mm, with compactment at 5000 kg/cm^2 load. The green samples were then sintered at a temperature of 1200 °C for 1 hour.

2.4. Characterization of nanocomposite SHF/COF

All samples were characterized using Permagraph (Magnet Physik, Germany) for the determination of magnetic properties. The morphology of the samples was then observed under a scanning electron microscope (SEM, JEOL-JSM IT-300 JAPAN). Subsequently, the phases present in each sample were identified with an X-ray diffractometer (Bruker D8 series) using Cu Kα (λ = 1.5418 Å) radiation.

3. Results and Discussions

3.1. Phase and structural analysis

XRD curves of diffraction patterns of SHF, COF, and the composites, namely S70C30, S75C25, S80C20, and S85C15 are presented in Fig. 1. The diffraction patterns of SHF and COF showed that both samples were single-phase crystalline materials, where $SrFe_{12}O_{19}$ (a) and $CoFe_2O_4$ (b) were the main phases. The diffraction pattern

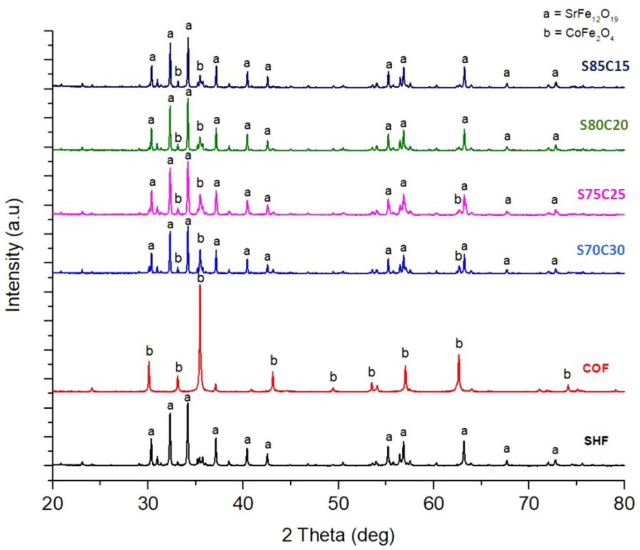

Fig. 1. (Color online) XRD pattern of SHF, COF, and composites.

of the composite samples was similar as it showed a mixed pattern of the original phase of SHF (a) and COF (b), as shown in Fig. 1. Based on this finding, the two main phases were identifiable in the diffraction pattern of the composite with no emergence of any additional diffraction peaks. The results showed that SHF (a) patterns were higher compared to COF (b) since the SHF content was greater. A low COF content led to a decrease in the intensity of peaks b, as seen at angles 2 Theta (~36° and ~63°). The diffraction pattern of SHF/COF nanocomposite samples with exchange spring interaction obtained from a simple solid-state reaction during 8 hours was shown by Hilczer *et al*. [12]. The nanocomposite also consisted of a mixed pattern of the two phases in all samples with the mass ratio ranging from 3:1 to 1:3.

Table 1. Summary of XRD quantitative analysis of SHF/COF nanocomposite samples.

Samples	Phase	Wt. %	Lattice Constant [Å]			Crystallite Size (nm)
			a	b	c	
SHF	$SrFe_{12}O_{19}$	100	5.880985	5.880985	23.055000	66
S70C30	$SrFe_{12}O_{19}$	80.9	5.876937	5.876937	23.062890	55
	$CoFe_2O_4$	19.1	8.375154	8.375154	8.375154	25
S75C25	$SrFe_{12}O_{19}$	87.5	5.876939	5.876939	23.062780	52
	$CoFe_2O_4$	12.5	8.376516	8.376516	8.376516	25
S80C20	$SrFe_{12}O_{19}$	91.3	5.877297	5.877297	23.061800	48
	$CoFe_2O_4$	8.7	8.377683	8.377683	8.377683	22
S85C15	$SrFe_{12}O_{19}$	92.7	5.877972	5.877972	23.061600	40
	$CoFe_2O_4$	7.3	8.377693	8.377693	8.377643	20
COF	$CoFe_2O_4$	100	8.380270	8.380270	8.380270	66

The summary of the XRD data analysis from all samples included phase, mass fraction, lattice parameter, and crystallite size, as shown in Table 1. The quantitative analysis results of phases in the composite samples showed variation in the phase content. The mass fraction of SHF phase was larger compared to its designation based on calculation. Furthermore, the mass fraction of COF was lower than its designated composition due to the interacting effect between COF and SHF phase during sintering treatment. Crystallite size measurements were obtained with the Williamson-Hall (W-H) analysis method using X-ray diffraction (XRD) data. This was carried out based on the analysis of the broadening of the diffraction peaks, which was obtained from the finite size of the crystallites. The results showed that the difference in composition affected both properties.

The SEM images of fracture surfaces for SHF (a) and COF (b) magnets showed the presence of grains aggregate, as shown in Fig. 2. The aggregate size of SHF was slightly lower compared to that of COF at approximately 1 μm. After the calcination treatment, compacting, and sintering for densification, agglomeration and grain growth occurred with less uniform grain size. Grain growth was due to mass transportation between particles, which was dominated by grain boundary and bimodal diffusion mechanism on the lattice [13]. The image of the fracture surface of the SHF sample indicated a more compact structure compared to COF.

SEM images of composite samples for S70C30 (a), S75C25 (b), S80C20 (c), and S85C15 (d) are presented in Fig. 3. The microstructure of composites consisted of hexagonal and spinel morphology. Furthermore, the two types of aggregates appeared to be oriented side by side and randomly in the composite sample with the shape and grain size of each unchanged. More grains were oriented side by side, causing intimate contact and exchange of magnetic springs between the two aggregates. The microstructure of the composites was more uniform compared to the single structure of SHF and COF. This was because the mixtures were ultrasonically processed for an hour before the compacting process. The higher the COF content, the more the probability of the spinel structure being in the composite morphology, and the hexagonal structure slightly closed in Fig. 3(a), (b), (c), and (d). The magnetic properties were highly dependent on the microstructure, hence, they were determined by the property of SHF and the spinel COF.

A full loop hysteresis compared the second quadrant curve of SHF, COF, and composite samples from which the M_r to M_s ratio determined the magnetic properties, such as H_c, M_r, and squareness as shown in Fig. 4. The SHF curve represented the characteristics of hard magnets with a high coercivity value (H_c = 3.30 kOe) and COF with soft magnetic behavior at a high magnetization saturation value (M_s = 71.11 emu/g) and magnetization of remanent value (M_r = 35.53 emu/g). The composite of hard and soft magnetic phases was one of the ways to improve magnetic properties [14]. When the hard and soft magnetic phases were in intimate contact in the composite structure, the effect of a magnetic exchange spring increased the values of M_s, M_r, and $(BH)_{max}$. However, the exchange spring effect was effective when the exchange length [15, 16] of the magnetic phase was larger than the mean grain size. Exchange length (L_{ex}) referred to the length of grain exchange interactions possessed by a material, and it varied among the samples. According to Herzer, L_{ex} could be calculated using the following equations (1) and (2) [17]:

$$L_{ex} = \sqrt{\frac{2A}{K_1}} \tag{1}$$

$K_1 = ½\ \mu_o M_s^2$, the equation (1) become (2):

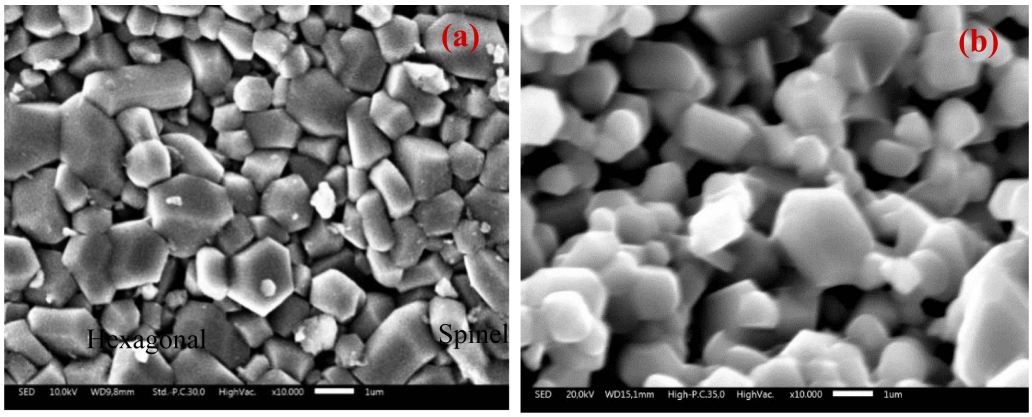

Fig. 2. (Color online) SEM images of fracture surfaces for (a) SHF and (b) COF.

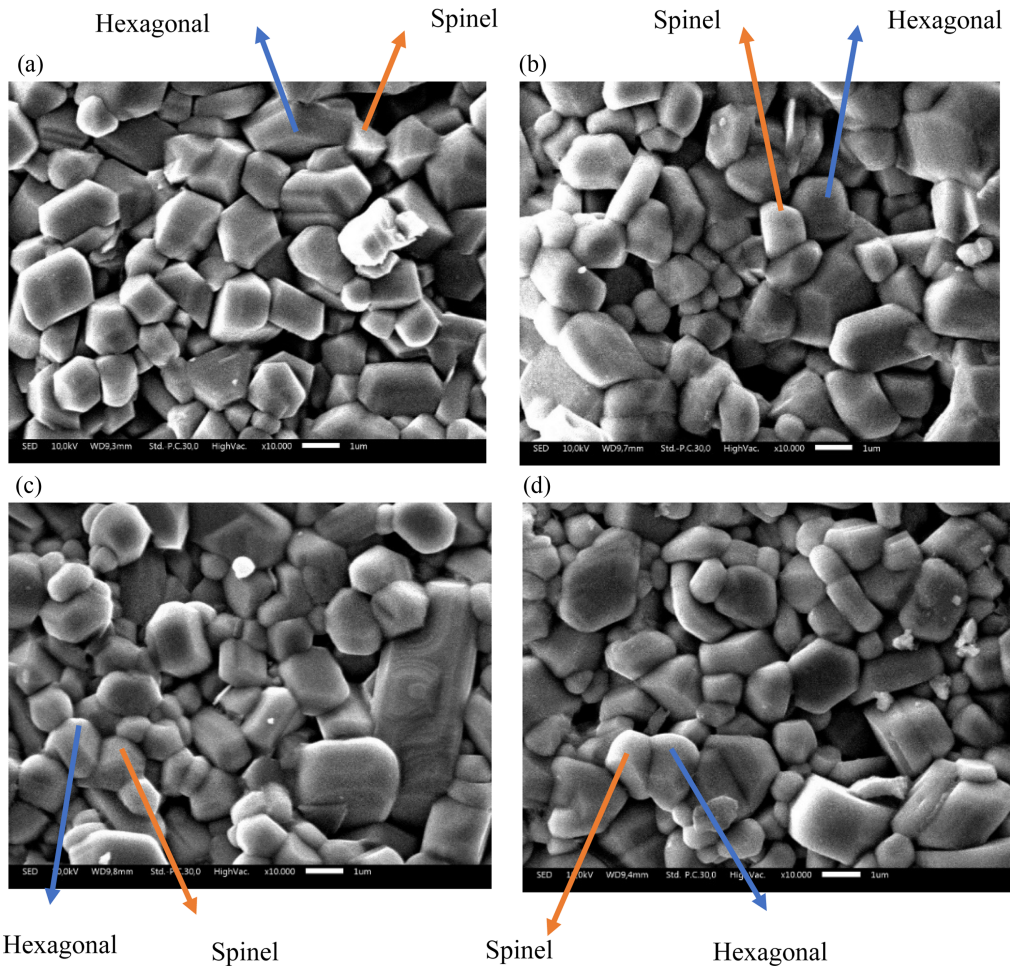

Fig. 3. (Color online) SEM images of the composites (a) S70C30, (b) S75C25, (c) S80C20, and (d) S85C15.

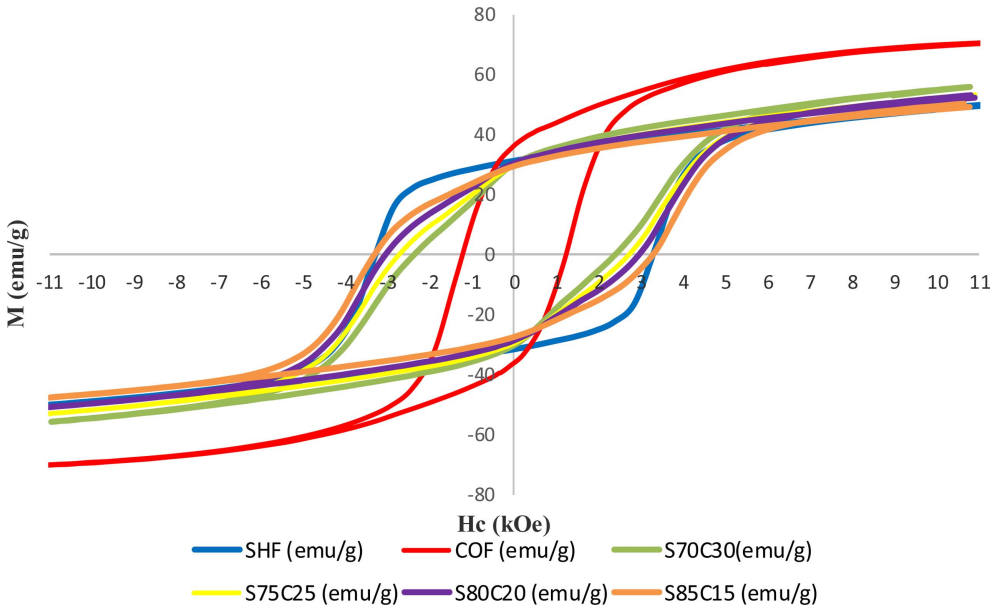

Fig. 4. (Color online) Full hysteresis loop of SHF, COF, and composites.

$$L_{ex} = \sqrt{\frac{2A}{\mu_0 Ms^2}} \quad (2)$$

Where A is exchange stiffness constant and K_1 is anisotropy constant. The theoretical values of A and K_1 for the material SHF = 6×10^{-12} J/m and 3.6×10^5 J/m^3 [18]. Theoretical values of A and K_1 for COF = 1×10^{-11} J/m and $2{,}7 \times 10^5$ J/m^3 [18]. μ_0 is the permeability of vacuum = $4\pi \times 10^{-7}$ H/m. From these theoretical values, when included in equation (2), the L_{ex} value for SHF and COF was approximately 10.60 nm and 11.58 nm, respectively. Based on these values, each SHF and COF item had a comparable length to ensure the items could interact with the same interaction distance [19]. The calculating result of the exchange length of the SHF/COF composite magnet ranged between the values obtained for SHF and COF. This indicated that the interaction between grains became effective in having an effect if the ratio of the area of interaction (s) and volume (v), namely (s/v) of grain, was relatively large. The finer the grain size of each component of the composite material, the greater the (s/v) ratio value. This was what underlied the investigation of the SHF/COF composite magnets. The variation in the s/v value of the composite magnet was obtained from the composition ratio of the composite. The results of the exchange length calculation are summarized in Table 2.

Table 2. The results of the exchange length of SHF, COF, and composite magnets.

Sample	Exchange length (nm)
SHF	10.60
S70C30	10.95
S75C25	11.76
S80C20	11.68
S85C15	11.65
COF	11.58

Table 3. Summary of quantitative analysis results of XRD data for SHF, COF, and composite magnets.

Sample	M_r (emu/g)	M_s (emu/g)	M_r/M_s	H_c (kOe)	$(BH)_{max}$ (MGOe)
SHF	31.73	51.31	0.62	3.30	0.92
S70C30	30.67	55.84	0.55	2.42	0.62
S75C25	30.25	53.32	0.57	2.87	0.59
S80C20	31.56	52.39	0.60	3.27	0.60
S85C15	30.39	52.02	0.58	3.32	0.68
COF	35.53	71.11	0.50	1.39	0.45

The exchange length was dependent on the microstructure, grain size, shape, synthesis method, and the distribution of hard and soft magnetic phases [20, 21]. In this study, the exchange spring magnet was influenced by the distribution of hard and soft magnetic phases with varying compositions. The hysteresis curves of the composite samples were between the SHF and COF curves. Differences in composition affected the magnetic characteristics of composite samples. Furthermore, M_s of the composites increased compared to a single SHF and its value was between the SHF and COF characteristic. This was due to the soft magnetic phase of COF providing a high magnetization of saturation and contributing to improving the M_s value of the samples.

The highest H_c and $(BH)_{max}$ value at S85C15 was obtained when the composition of SHF was high. The values of M_r, H_c, and $(BH)_{max}$ also increased compared to the magnetic characteristics of a single COF. All composites had a M_r/M_s ratio of more than 0.5, and when it exceeded the theoretical limit of 0.5, there was an exchange spring magnet. All magnetic properties are summarized in Table 3.

4. Conclusion

In conclusion, exchange spring magnetic occurred in the SHF/COF nanocomposites due to different compositions (70:30, 75:25, 80:20, 85:15), which affected the phase, morphology, and magnetic properties. Furthermore, the original SHF and COF existed in all XRD patterns without the emergence of additional diffraction peaks. The morphology of composite magnets consisted of hexagonal and cubic structures that were dispersed across all composite samples. Magnetic properties of the composite, namely M_s, H_c, and $(BH)_{max}$ values were between SHF and single COF. The addition of SHF content increased the H_c obtained, and the highest value was recorded in sample S85C15. All the M_r/M_s ratio values in this study were above the theoretical limit of single-phase SHF which indicates that there had been an exchange spring magnet in SHF/COF nanocomposites with various composition ratios.

Acknowledgment

This study was supported by the HOUSE Program 2022. The authors are grateful to the Research Organization of Nanotechnology and Materials as well as the Research Centre for Advanced Materials, the National Research and Innovation Agency.

References

[1] Y. Haibo, L. Miao, L. Ying, D. Guoqiang, H. Lingyan, and T. Jingyi, Mater. Chem. Phys. **160**, 11 (2015).
[2] R. Debangsu and K. Anil, J. Appl. Phys. **073902**, 1 (2010).
[3] M. Radmanesh and S. Ebrahimi, J Supercond Nov Magn. **2411** (2013).
[4] N. Hossein, M. Mahmood, K. Parviz, and H. B. Gholam, J. Electron. Mater (2017).
[5] T. Schrefl, H. Kronmiiller, and J. Fidler, J. Magn. Magn. Mater **127** (1993).
[6] M. Liu, H. Yang, Y. Lin, and Y. Yang, Mater. Res. Bull **60** (2014).
[7] J. S. Jiang, Appl. Phys. Lett. **5293** (2004).
[8] M. A. Moskalenko, V. M. Uzdin, H. Zabel, M. A. Moskalenko, V. M. Uzdin, and H. Zabel, J. Appl. Phys. **053913** (2014).
[9] J. H. Yin, J. Appl. Phys. **85** (1999).
[10] J. O. Yang, Ceram. Int. **41** (2015).
[11] S. D. Bader, Rev. Mod. Phys. **78** (2006).
[12] A. Hilczer, K. Kowalska, E. Markiewicz, and A. Pietraszko, Mater. Sci. Eng. **207** (2016).
[13] S. A. Ali, M. A. Matin, M. A. Hakim, and M. F. Islam, IOP Conf. Ser. Mater. Sci. Eng. Pap. (2018).
[14] Y. Cedeño-mattei, O. Perales-pérez, and O. N. C. Uwakweh, J. Magn. Magn. Mater. **341** (2013).
[15] H. Yang, T. Ye, Y. Lin, M. Liu, G. Zhang, and P. Kang, Mater. Lett. **171** (2015).
[16] S. Singh, S. Munjal, and N. Khare, J. Magn. Magn. Mater. **386** (2015).
[17] G. S. Abo, Y. Hong, J. Park, J. Lee, W. Lee, and B. Choi, IEEE Trans. Magn. **49** (2013).
[18] P. Jing and Q. Liu, Scientific Reports **5** (2015).
[19] Y. Melikhov, J. Appl. Phys. **102** (2006).
[20] R. Skomski and J. Zhou, Nanomagnetic Models, University of Nebraska, Lincoln, USA (2006) pp 41-90.
[21] F. Song, X. Shen, M. Liu, and J. Xiang, J. Solid State Chem. **185** (2012).